Supporting information for

# *Operando* Identification of the Dynamic Behavior of Oxygen Vacancy-Rich $Co_3O_4$ for Oxygen Evolution Reaction

Zhaohui Xiao, Yu-Cheng Huang, Chung-Li Dong, Chao Xie, Zhijuan Liu, Shiqian Du, Wei Chen, Dafeng Yan, Li Tao, Zhiwen Shu, Guanhua Zhang, Huigao Duan, Yanyong Wang, Yuqin Zou, Ru Chen, and Shuangyin Wang*

**Experimental.**

Samples preparation. According to previous reports,[1] we did a little optimizing in parameters. The pure $Co_3O_4$ nanosheet arrays were prepared by the electrodeposition method in three-electrodes cell with Ti foil (or carbon paper) as working electrode and counter electrode, and saturated calomel electrode (SCE) as reference electrode at room temperature. The $Co(OH)_2$ was electrodeposited in a 0.05 M $Co(NO_3)_2$ aqueous electrolyte. The electrodeposition potential is -1.0 V (vs. SCE). After 10 minutes electrodeposition, the green $Co(OH)_2$ sample was obtain and then to be calcined at 250 °C for 2 hours with a heating rate of 1°C $min^{-1}$ to transform into $Co_3O_4$. The mass loading of $Co_3O_4$ on matrix (Ti foil or carbon paper) was around 0.5 mg $cm^{-2}$. The $Co_3O_4$ nanosheets array was treated by Ar plasma (commercial 13.56 MHz RF source, 250W and 100 Pa) with 120 s to obtain plasma-engraved $Co_3O_4$ ($V_O$-$Co_3O_4$) for next detailed studies.

Characterization. Surface morphology of all catalysts was characterized by field-emission scanning electron microscope (SEM, Carl-Zeiss, SIGMA HD) and transmission electron microscopy (TEM, Tecnai G2 F20 and JEM-2100Plus). The surface area was measured by nitrogen adsorption-desorption isotherms using the Brunauer Emmett Teller (BET) method on a Micromeritics ASAP 2020 V3.02 H. The X-ray photoelectron spectroscopy (XPS, Thermo, ESCALAB 250XI and SHIMADZU-KRATOS, AXIS SUPRA) were carried out to obtain surfaces structural information and properties of the catalysts. The spectra were normalized by the same maximum of the intensity. XPS binding energies (BE) were reported referenced to the C 1s line at 284.8 eV BE for adventitious carbon. The crystal structures of the samples were characterized using powder X-ray diffraction (XRD, Bruker, D8 Advance). The Raman spectra were collected on a Raman spectrometer (Raman, Labram-010) using a 632 nm laser and the power was 2mW. Electron paramagnetic resonance (EPR) spectra were performed using a Bruker ESR spectrometer (JES-FA200). Zeta potential was measured on a Malvern Zetasizer Nano series analyser (Zetasizer Nano ZS) in deionized water. The *operando* synchrotron X-ray absorption spectroscopy (XAS) were obtained by beamline TPS44A (Quick-scanning XAS, transmission mode) at the National Synchrotron Radiation Research Center (NSRRC, Taiwan).

Electrochemical measurements. Electrochemical experiments were performed in a typical three-electrode system controlled using a CHI-760E (CHI Instruments). Before the electrochemical measurement, the electrolyte was degassed by bubbling oxygen for at least 30 min to achieve a saturation condition of oxygen gas. All potentials were referenced to an SCE reference electrode, and carbon rod was used as the counter electrode in all measurements. All electrochemical was presented without *IR*-correction unless otherwise specified. The SCE reference electrode was calibrated before OER measurements,[2,3] and the calibration equation: $E_{RHE} = E_{SCE} + 1.05$ V, in 1 M KOH; $E_{RHE} = E_{SCE} + 0.99$ V, in 0.1 M KOH; $E_{RHE} = E_{SCE} + 0.655$ V, in 0.1 M PBS. Cyclic voltammetry (CV) measurements set 10 mV $s^{-1}$. *Operando* characterization tandem electrochemical operation were carried out specify potential for 10 min to obtain the surface chemical composition and structural information of materials. Electrochemical impedance spectroscopy (EIS) tests were performed at different applied potentials versus RHE in the frequency range of 0.01-100000 Hz.

**Supporting Figures.**

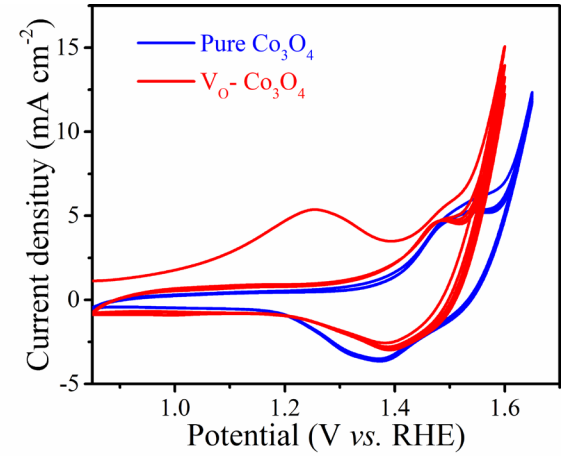


Figure S1. CVs measured (five cycles) for pure $Co_3O_4$ and $V_O$-$Co_3O_4$ in 1 M KOH.

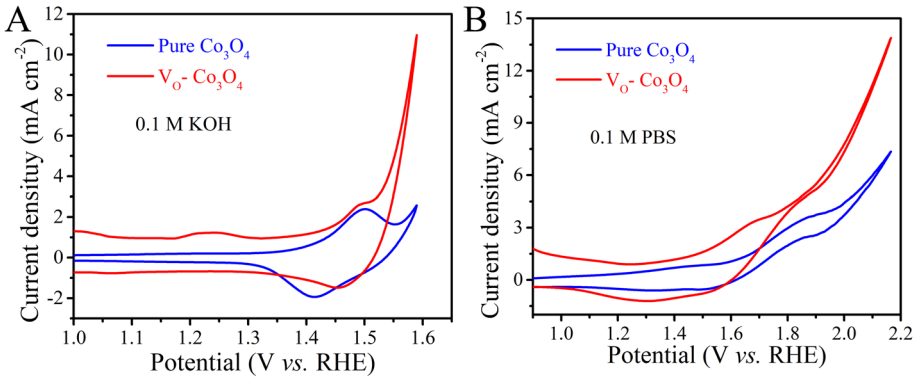


Figure S2. CVs measured for pure $Co_3O_4$ and $V_O$-$Co_3O_4$ in 0.1 M KOH (A) and 0.1 M PBS (B).

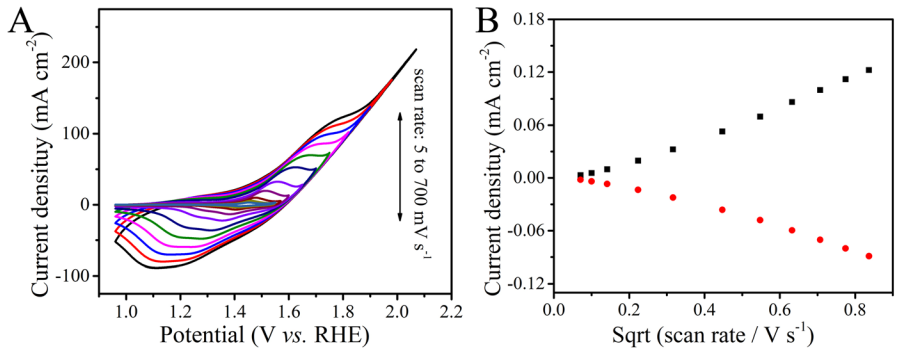


Figure S3. Analysis of pure $Co_3O_4$ in Laviron equation. (A) CVs of pure $Co_3O_4$ with scan rates from 5, 10, 20, 50, 100, 200, 300, 400, 500, 600 to 700 mV $s^{-1}$, 1 M KOH. (B) The plot of the redox peak currents densities versus the square root of scan rates.

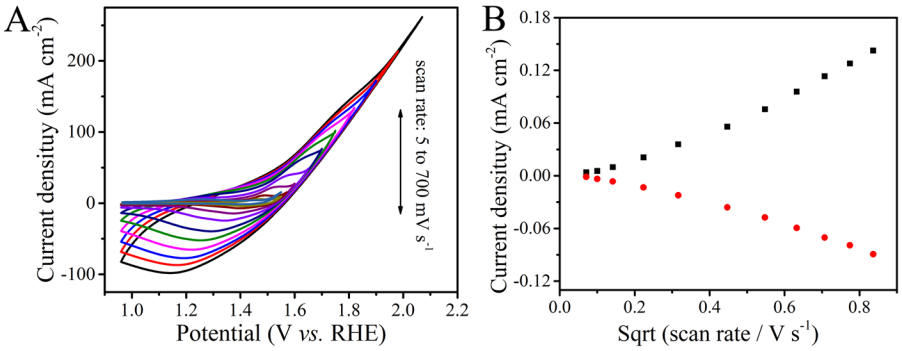


Figure S4. Analysis of $V_O$-$Co_3O_4$ in Laviron equation. (A) CVs of $V_O$-$Co_3O_4$ with scan rates from 5, 10, 20, 50, 100, 200, 300, 400, 500, 600 to 700 mV $s^{-1}$, 1 M KOH. (B) The plot of the redox peak currents densities versus the square root of scan rates.

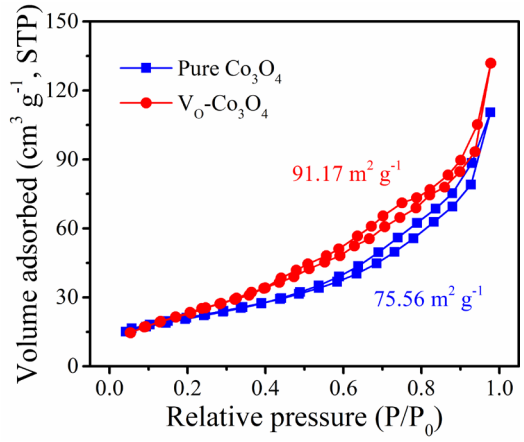


Figure S5. BET of pure $Co_3O_4$ (A) and $V_O$-$Co_3O_4$ (B) as prepared.

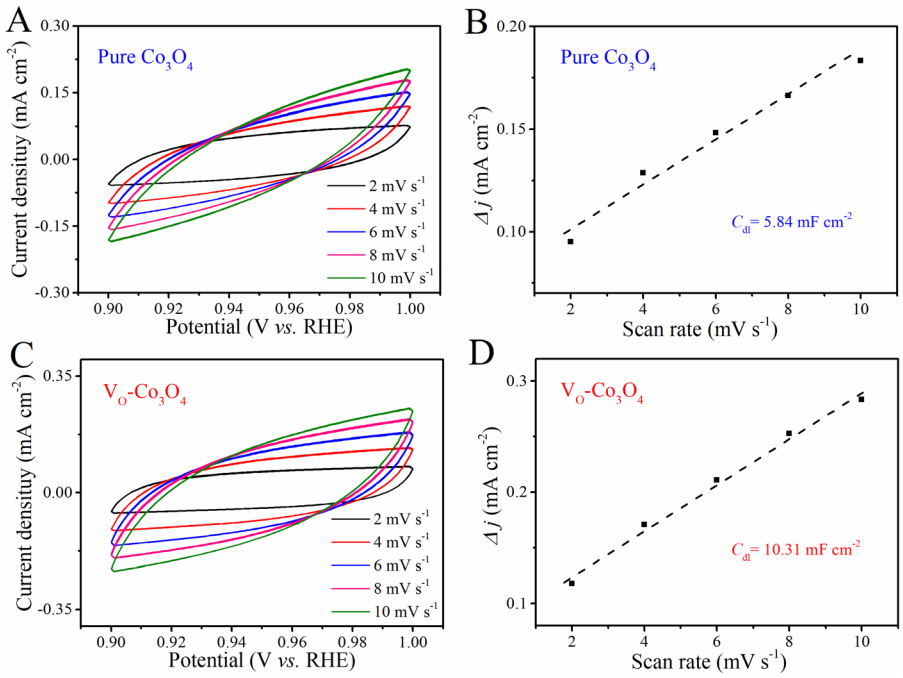


Figure S6. ECSA test for pure $Co_3O_4$ and $V_O$-$Co_3O_4$. CV curves (A, C) and $C_{dl}$ (B, D) of pure $Co_3O_4$ and $V_O$-$Co_3O_4$, respectively.

Note: The electrochemical active surface area (ECSA) was estimated by measuring the capacitive current associated with double-layer charging from the scan-rate dependence of cyclic voltammograms (CVs), according to the previous literature.[4,5] The potential window of CVs of two $Co_3O_4$ samples were 0.9 ~1.0 V (*vs*. RHE, Figure S6) in a non-Faradaic potential range under different scan rates with 2, 4, 6, 8 and 10 mV $s^{-1}$. The double layer capacitances ($C_{dl}$) of two $Co_3O_4$ samples were estimated by plotting the $\Delta J = J_a - J_c$ at 0.95 V (*vs*. RHE) against the scan rate. The linear slope is equivalent to twice of the double-layer capacitance $C_{dl,}$ and the electrochemical active surface area (ECSA) of catalyst was calculated by the following equation:

$$ECSA = C_{dl}/C_s$$

Where $C_s$ is the specific capacitance of planar surface with a atomically smooth under identical electrolyte conditions. We use general value of 40 μF $cm^{-2}$.[5]

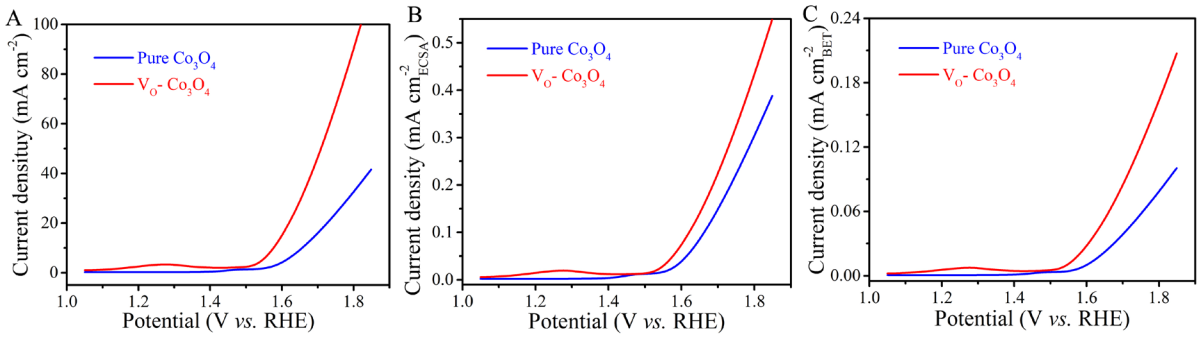


Figure S7. (A) First LSV polarization curves (without *IR*-correction) of pure $Co_3O_4$ and $V_O$-$Co_3O_4$. LSV polarization curves of pure $Co_3O_4$ and $V_O$-$Co_3O_4$ after normalized by ECSA (B) and BET (C).

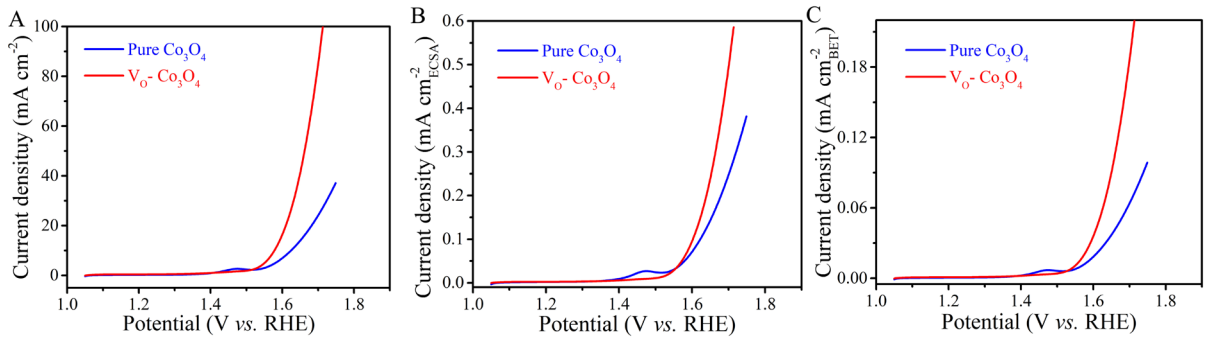


Figure S8. (A) LSV polarization curves (with *IR*-correction) of pure $Co_3O_4$ and $V_O$-$Co_3O_4$ after five CVs test. LSV polarization curves of pure $Co_3O_4$ and $V_O$-$Co_3O_4$ after normalized by ECSA (B) and BET (C).

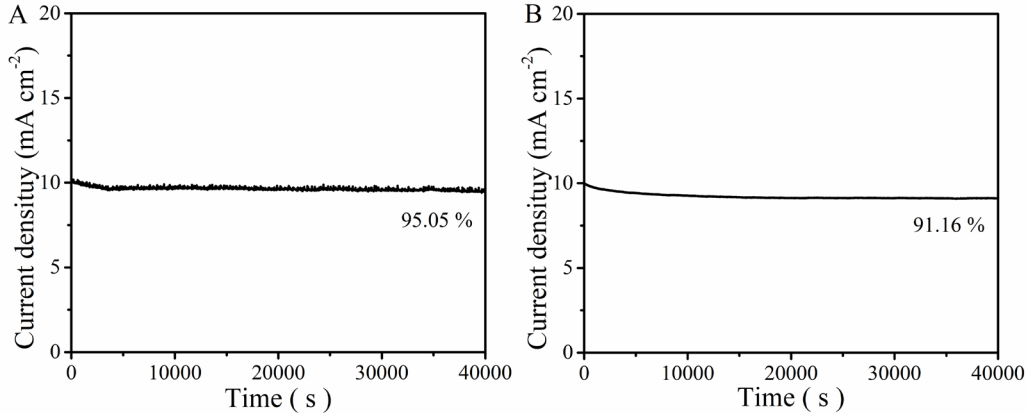


Figure S9. Stability of pure $Co_3O_4$ (A) and $V_O$-$Co_3O_4$ (B), respectively.

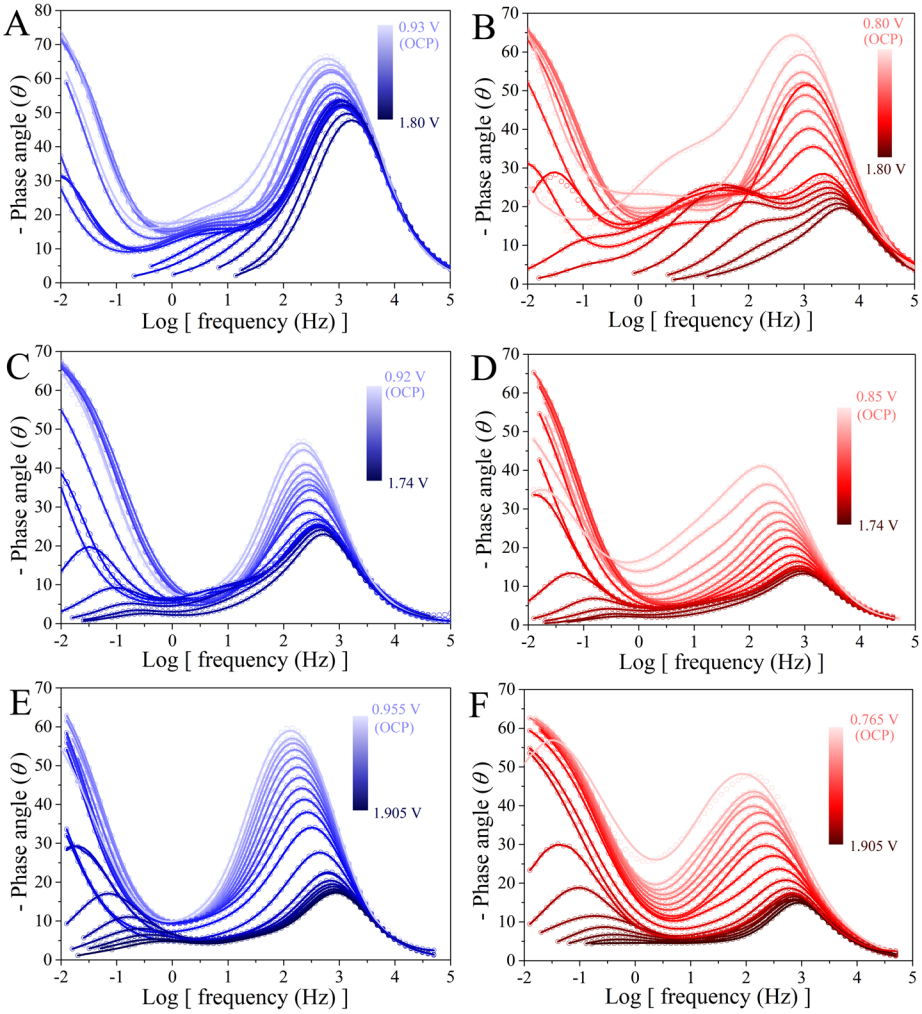


Figure S10. Bode phase plots of pure $Co_3O_4$ (A, C, E) and $V_O$-$Co_3O_4$ (B, D, F) in this work to applied potential in the solution of 1 M KOH, 0.1 M KOH and 0.1 M PBS. Open circles were test data points and solid lines were corresponding fitting.

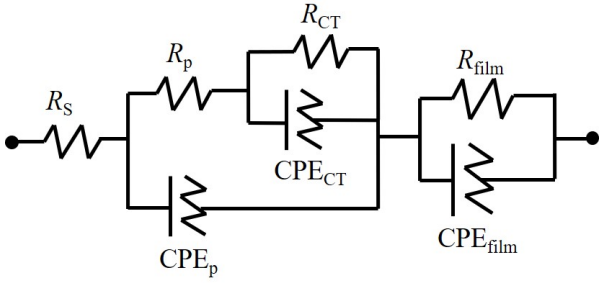


Figure S11. The equivalent circuit used for modeling the measured electrochemical response. $CPE_{film}$ and $R_{film}$ are represented as the dielectric property and resistance of catalyst film, respectively. $CPE_p$ is related to double layered capacitance and $CPE_{CT}$ models the relaxation of the charge associated with the adsorbed intermediate. $R_{CT}$ and $R_p$ are related with the kinetics of the interfacial charge transfer reaction, $R_s$ represents solution resistance.[6,7]

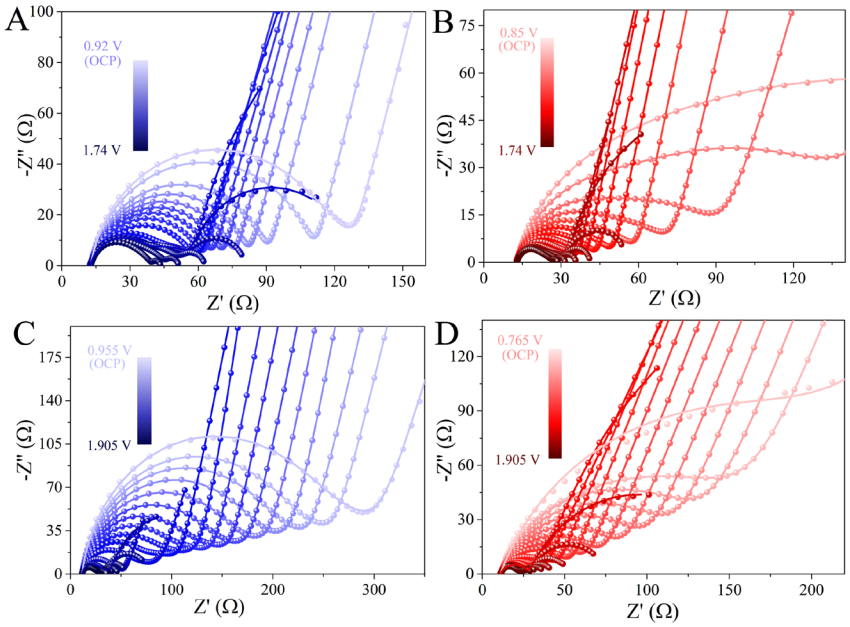


Figure S12. Nyquist plots for (A, C) pure $Co_3O_4$ and (B, D) $V_O$-$Co_3O_4$ catalysts at different applied potentials versus RHE in 0.1 M KOH and 0. M PBS, respectively. Globules were test data points and solid lines were corresponding fitting.

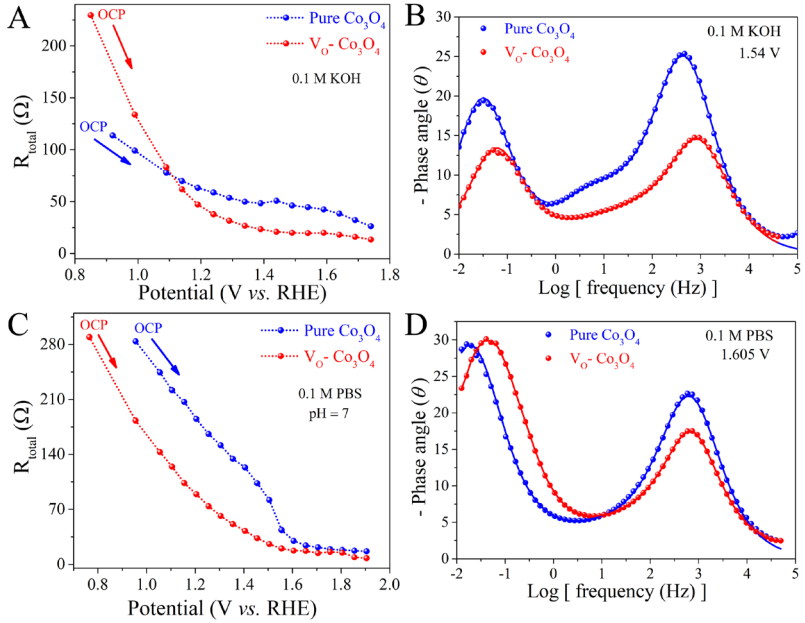


Figure S13. Response of the total charge transfer resistance ($R_{total}$) to applied potential of the catalysts studied to applied potential in 0.1 M KOH (A) and 0.1 M PBS (C) for pure $Co_3O_4$ and $V_O$-$Co_3O_4$. Bode phase plots of pure $Co_3O_4$ and $V_O$-$Co_3O_4$ at 1.605 V *vs.* RHE in 0.1 M KOH (B) and at 1.54 V *vs.* RHE in 0.1 M PBS (D). Globules were test data points and solid lines were corresponding fitting. Dotted lines were to guide the eye.

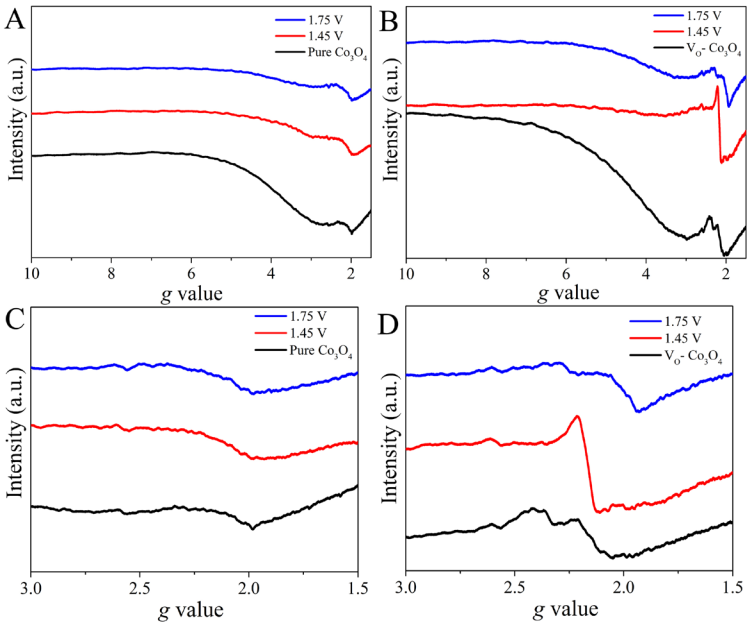


Figure S14. EPR spectra of pure $Co_3O_4$ (A) and $V_O$-$Co_3O_4$ (B) were carried out the critical potential. (C) and (D) were the local enlarged figure in (A) and (B), respectively.

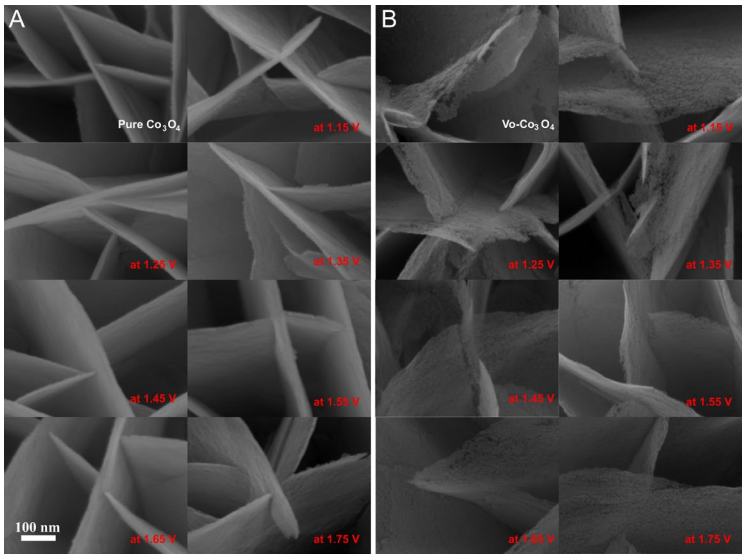


Figure S15. SEM for pure $Co_3O_4$ (A) and $V_O$-$Co_3O_4$ (B) were carried out the applied potential.

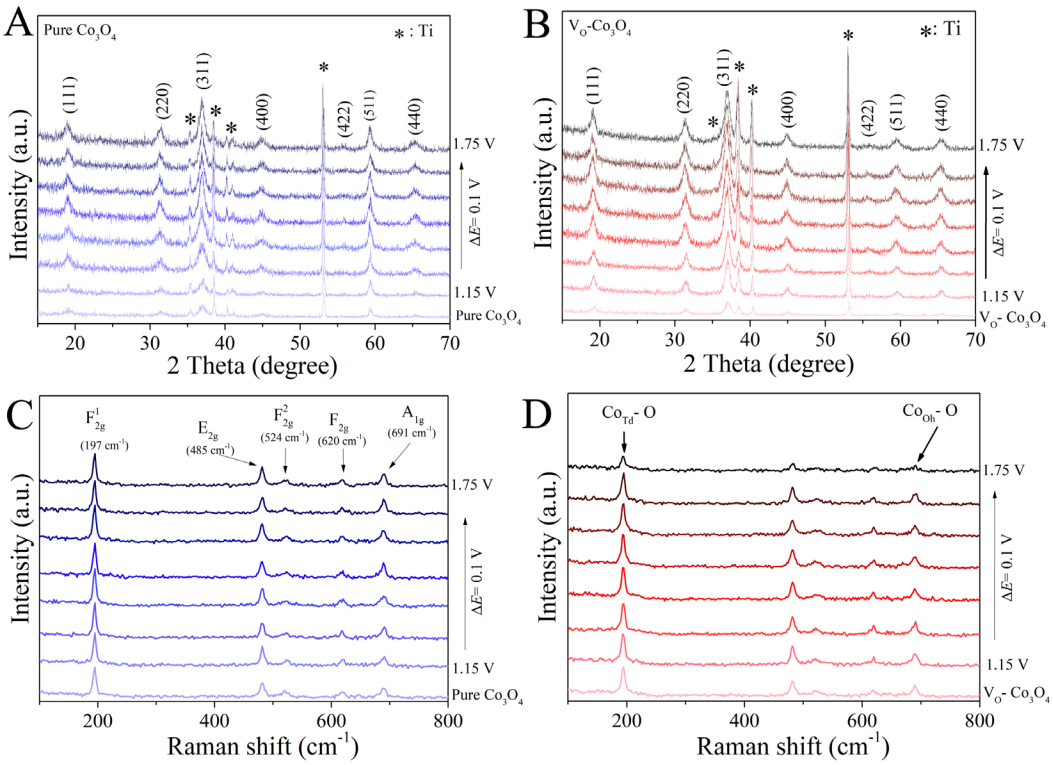


Figure S16. XRD and Raman for pure $Co_3O_4$ and $V_O$-$Co_3O_4$ were carried out the applied potential.

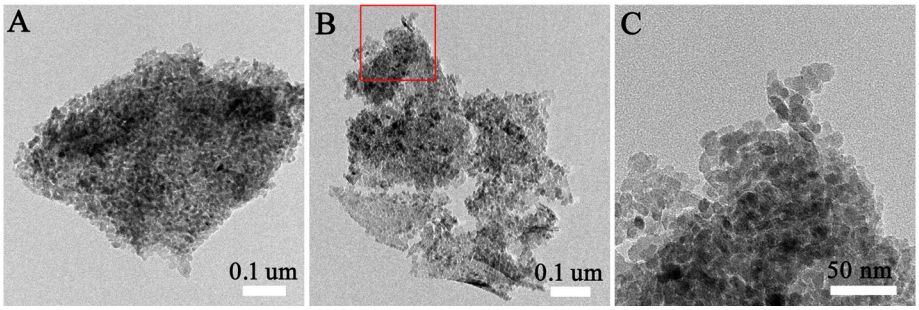


Figure S17. TEM of (A) pure $Co_3O_4$ and (B) $V_O$-$Co_3O_4$, respectively. (C) was local enlarged of the red box in (A).

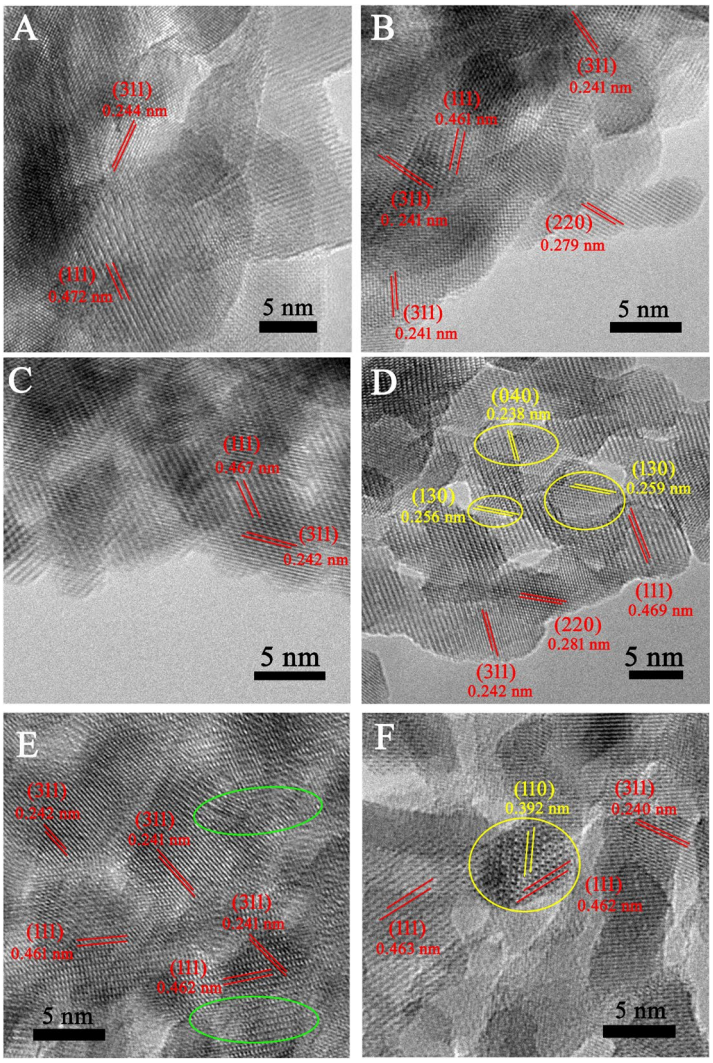


Figure S18. HRTEM of (A, C, E) pure $Co_3O_4$ and (B, D, F) $V_O$-$Co_3O_4$, respectively. (A) and (B) were samples as prepared, (C) and (D) were samples after five CVs test, (E) and (F) were samples after 40000s test. The green circles in (E) indicated some lattice disorder, the yellow circles in (D) and (F) indicated some typical planes in CoOOH (PDF: 26-0480). The red stripe indicated the various crystal faces of spinel $Co_3O_4$ (PDF: 43-1003).

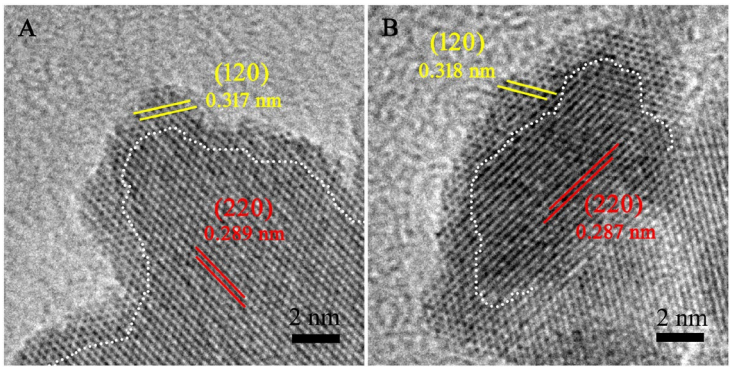


Figure S19. HRTEM of $V_O$-$Co_3O_4$ after five CVs (A) and 40000s test (B). The yellow stripe indicated (120) plane of CoOOH (PDF: 26-0480). The red stripe indicated (220) plane of spinel $Co_3O_4$. White dotted lines are to guide the eye.

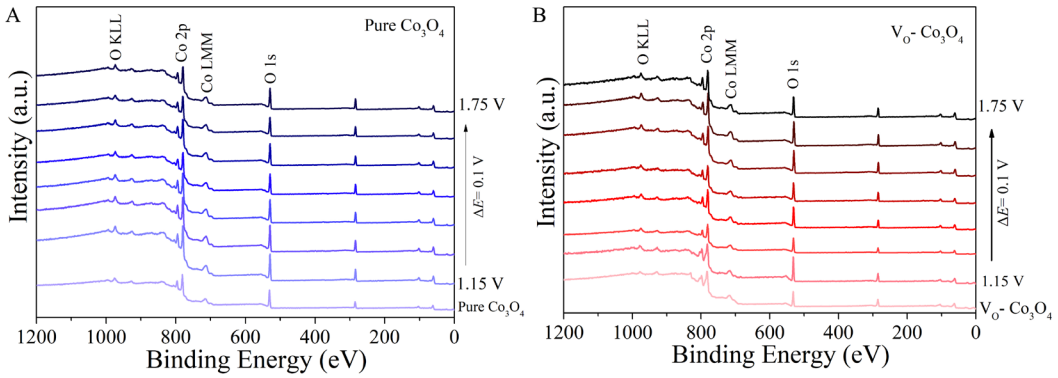


Figure S20. XPS for pure $Co_3O_4$ (A) and $V_O$-$Co_3O_4$ (B) were carried out the applied potential.

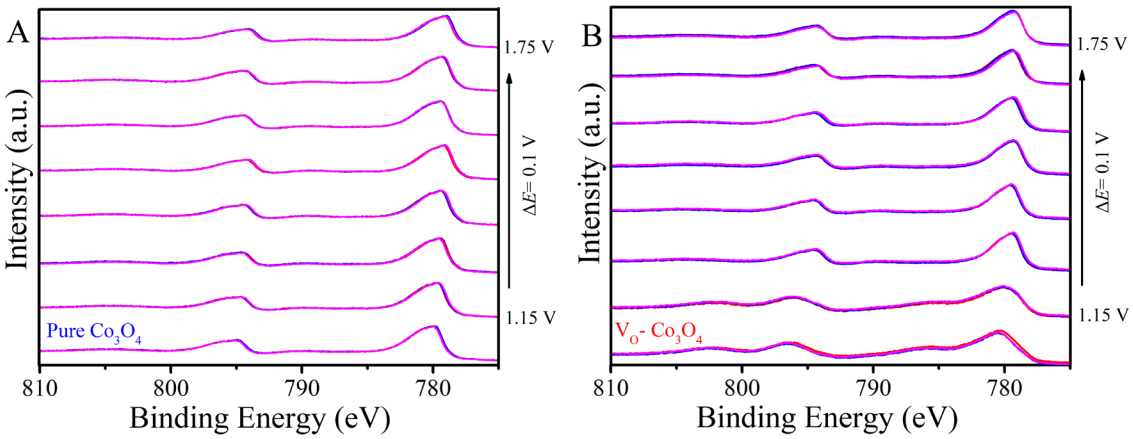


Figure S21. Three times Co 2p XPS spectrum were piled up for (A) pure $Co_3O_4$ and (B) $V_O$-$Co_3O_4$ in the applied potential, respectively.

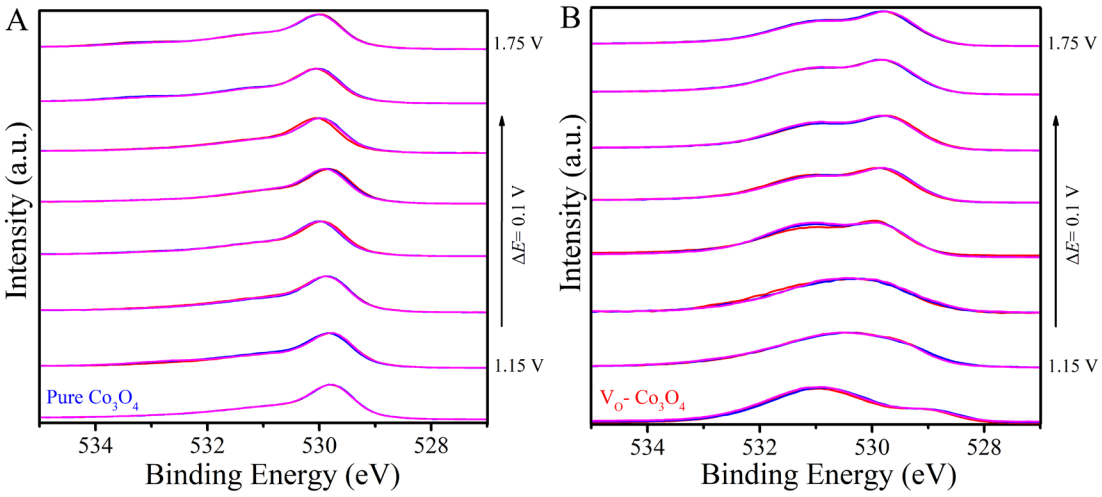


Figure S22. Three times O 1s XPS spectrum were piled up for (A) pure $Co_3O_4$ and (B) $V_O$-$Co_3O_4$ in the applied potential, respectively.

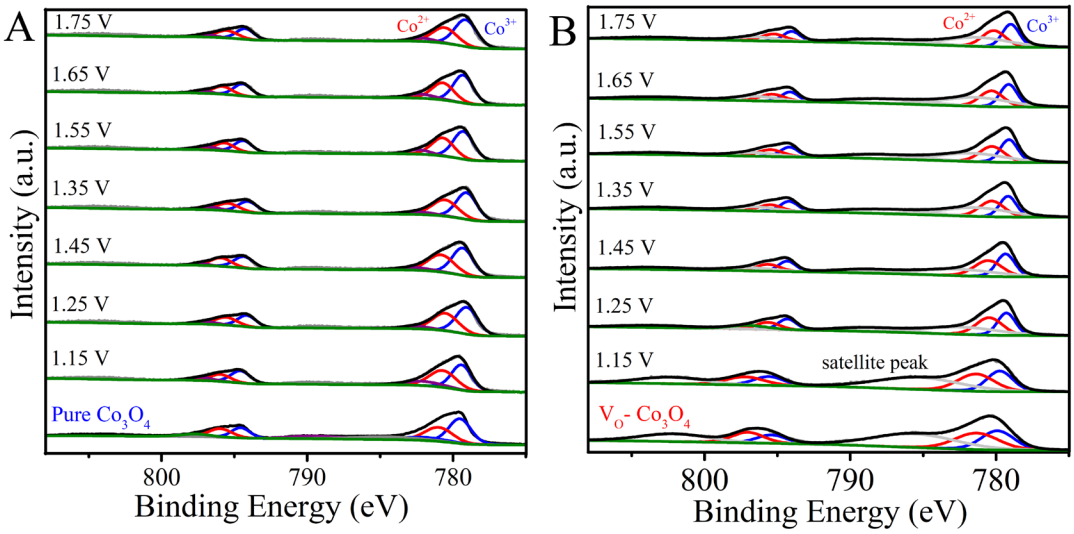


Figure S23. Co 2p XPS spectrum fitting for (A) pure $Co_3O_4$ and (B) $V_O$-$Co_3O_4$ were carried out the applied potential.

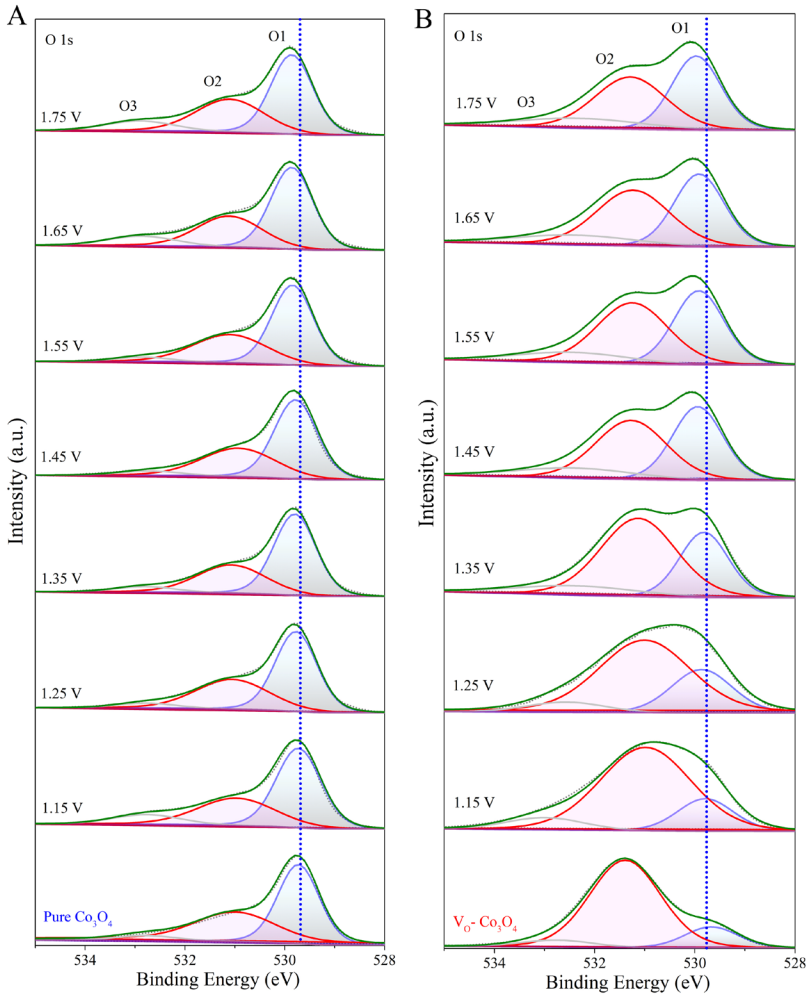


Figure S24. O 1s XPS spectrum fitting for (A) pure $Co_3O_4$ and (B) $V_O$-$Co_3O_4$. Dotted lines are to guide the eye.

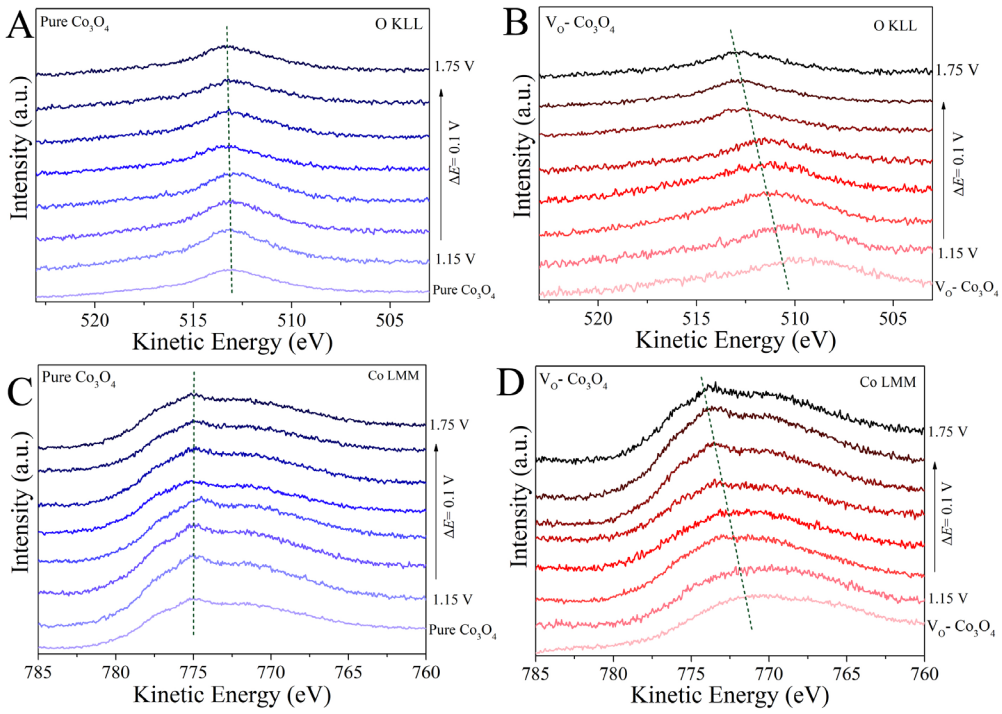


Figure S25. Auger spectra for pure $Co_3O_4$ (A, C) and $V_O$-$Co_3O_4$ (B, D) were carried out the applied potential. Dotted lines are to guide the eye.

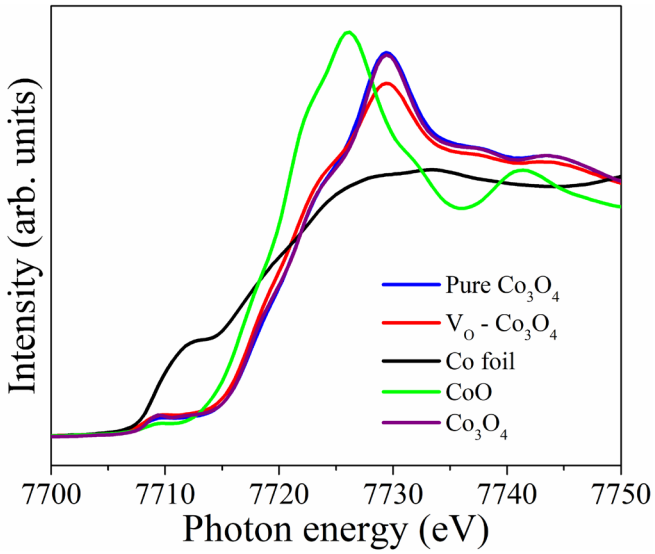


Figure S26. XAFS for Co K-edge of pure $Co_3O_4$, $V_O$-$Co_3O_4$ and three standards of cobalt-based materials.

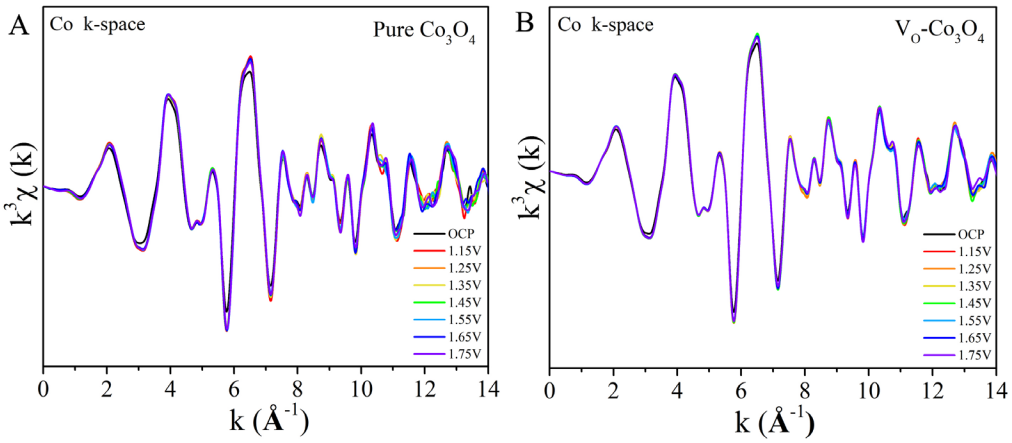


Figure S27. The *operando* $k^3$-weighted EXAFS for pure $Co_3O_4$ (A) and $V_O$-$Co_3O_4$ (B) in Co *K*-edge.

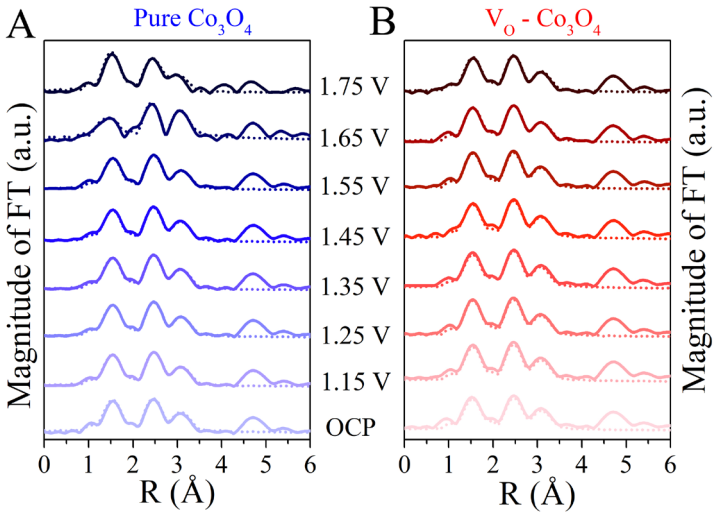


Figure S28. *Operando* EXAFS spectra were carried out the critical potential and the corresponding fitting for pure $Co_3O_4$ (A) and $V_O$-$Co_3O_4$ (B). Experimental data and fitted profiles were shown in bold and dot lines, respectively.

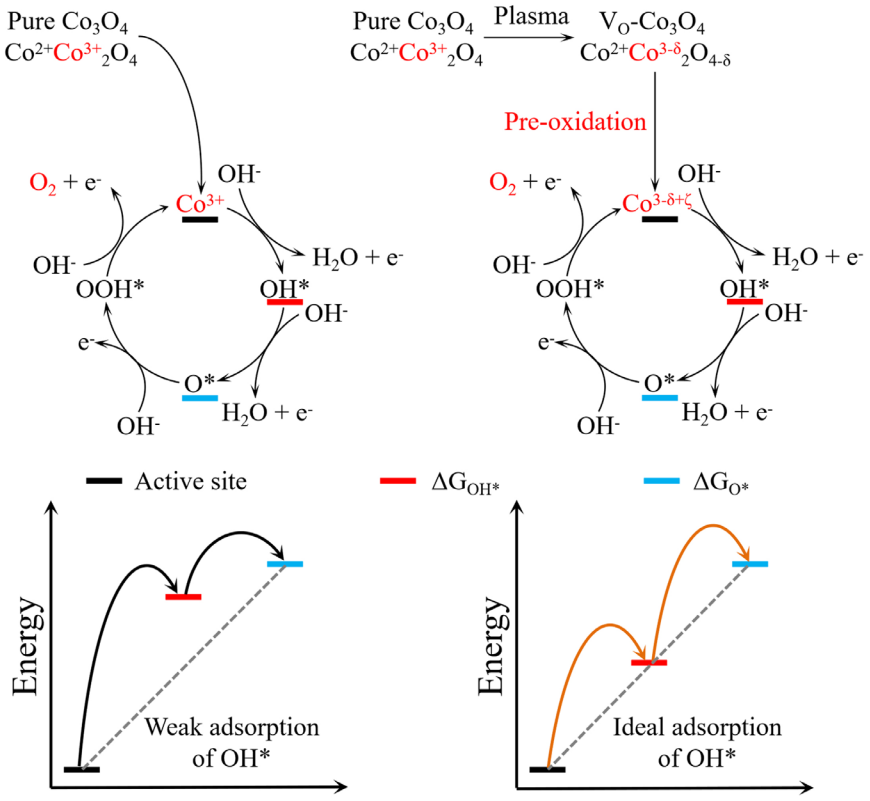


Figure S29. Schematic illustration of the Co sites with ideal adsorption energy of $OH^-$ by oxygen vacancy regulated.

**Supporting Table.**

Table S1. Summary of the impedance fitting data for pure $Co_3O_4$ electrode in 1 M KOH.

| Potential (V *vs.* RHE) | $R_S$ (Ω) | $R_p$ (Ω) | $CPE_p$ (mF) | $R_{film}$ (Ω) | $CPE_{film}$ (mF) | $R_{CT}$ (Ω) | $CPE_{CT}$ (mF) | $R_{total}$ (Ω) |
|---|---|---|---|---|---|---|---|---|
| 0.93 (OCP) | 1.9017 | 85.664 | 0.04276 | 152.61 | 1.3147 | - | 16.836 | 238.274 |
| 1.05 | 1.8955 | 66.570 | 0.04140 | 117.77 | 2.4619 | - | 17.853 | 184.340 |
| 1.15 | 1.8858 | 56.901 | 0.04207 | 73.693 | 3.6809 | - | 21.877 | 130.594 |
| 1.2 | 1.8724 | 53.953 | 0.04364 | 65.508 | 3.7421 | - | 22.878 | 119.461 |
| 1.25 | 1.8994 | 38.406 | 0.04576 | 67.501 | 2.9833 | - | 23.439 | 105.907 |
| 1.3 | 1.8961 | 35.952 | 0.04760 | 60.156 | 3.4098 | - | 28.896 | 96.108 |
| 1.35 | 1.889 | 31.837 | 0.04981 | 56.304 | 4.2881 | - | 59.184 | 88.141 |
| 1.4 | 1.8842 | 26.557 | 0.05057 | 54.170 | 5.8209 | - | 192.66 | 80.727 |
| 1.45 | 1.8794 | 23.924 | 0.05180 | 46.449 | 7.1184 | - | 315.338 | 70.373 |
| 1.5 | 1.8773 | 22.581 | 0.05273 | 39.828 | 6.3591 | 135.65 | 203.570 | 62.409 |
| 1.55 | 1.8794 | 23.007 | 0.05211 | 34.765 | 5.1814 | - | - | 57.772 |
| 1.6 | 1.8383 | 25.448 | 0.04916 | 28.933 | 4.1153 | - | - | 54.381 |
| 1.65 | 1.8338 | 26.078 | 0.05196 | 14.912 | 2.1751 | - | - | 40.990 |
| 1.7 | 1.8348 | 24.060 | 0.05199 | 6.5522 | 2.3287 | - | - | 30.612 |
| 1.75 | 1.8262 | 20.982 | 0.05473 | - | - | - | - | 20.982 |
| 1.8 | 1.8406 | 16.461 | 0.04488 | - | - | - | - | 16.461 |

Table S2. Summary of the impedance fitting data of $V_O$-$Co_3O_4$ electrode in 1 M KOH.

| Potential (V *vs.* RHE) | $R_S$ (Ω) | $R_p$ (Ω) | $CPE_p$ (mF) | $R_{film}$ (Ω) | $CPE_{film}$ (mF) | $R_{CT}$ (Ω) | $CPE_{CT}$ (mF) | $R_{total}$ (Ω) |
|---|---|---|---|---|---|---|---|---|
| 0.8 (OCP) | 1.6699 | 56.938 | 0.07221 | 314.630 | 0.62197 | - | 13.611 | 371.568 |
| 0.93 | 1.6656 | 47.203 | 0.06413 | 231.250 | 3.5579 | - | 1.2518 | 278.453 |
| 1.05 | 1.7308 | 39.053 | 0.04946 | 178.070 | 3.7614 | - | 25.174 | 217.123 |
| 1.15 | 1.7250 | 25.386 | 0.05253 | 108.850 | 7.2195 | - | 32.563 | 134.236 |
| 1.2 | 1.7169 | 20.749 | 0.06013 | 71.858 | 6.1459 | - | 28.841 | 92.607 |
| 1.25 | 1.7109 | 15.727 | 0.06707 | 55.582 | 5.6445 | - | 30.606 | 71.309 |
| 1.3 | 1.7060 | 11.346 | 0.07464 | 45.927 | 5.6341 | - | 38.423 | 57.273 |
| 1.35 | 1.7038 | 7.7660 | 0.07872 | 40.583 | 6.2846 | - | 60.518 | 48.349 |
| 1.4 | 1.7057 | 4.9908 | 0.07314 | 37.747 | 7.8629 | - | 127.96 | 42.738 |
| 1.45 | 1.7081 | 3.6581 | 0.06669 | 32.796 | 8.6284 | 413.470 | 168.45 | 36.454 |
| 1.5 | 1.5777 | 2.1876 | 0.09681 | 29.471 | 7.0068 | 68.505 | 131.3 | 31.659 |
| 1.55 | 1.6227 | 2.1334 | 0.11236 | 26.356 | 5.8473 | 13.025 | 148.83 | 28.489 |
| 1.6 | 1.6584 | 2.3221 | 0.13845 | 18.399 | 4.3117 | 2.4262 | 339.641 | 20.721 |
| 1.65 | 1.6785 | 2.2713 | 0.12887 | 9.3504 | 2.7954 | - | - | 11.622 |
| 1.7 | 1.6960 | 2.7569 | 0.09426 | 3.7239 | 2.3484 | - | - | 6.481 |
| 1.75 | 1.7064 | 2.4514 | 0.08115 | 1.6908 | 2.9049 | - | - | 4.142 |
| 1.8 | 1.7013 | 2.2873 | 0.08245 | 0.8372 | 4.3409 | - | - | 3.125 |

Table S3. Summary of the impedance fitting data for pure $Co_3O_4$ electrode in 0.1 M KOH.

| Potential (V *vs.* RHE) | $R_S$ (Ω) | $R_p$ (Ω) | $CPE_p$ (mF) | $R_{film}$ (Ω) | $CPE_{film}$ (mF) | $R_{CT}$ (Ω) | $CPE_{CT}$ (mF) | $R_{total}$ (Ω) |
|---|---|---|---|---|---|---|---|---|
| 0.92 (OCP) | 12.634 | 108.110 | 0.04861 | 5.512 | 0.00272 | - | 14.463 | 113.622 |
| 0.99 | 12.669 | 95.686 | 0.04906 | 3.399 | 0.00593 | - | 16.266 | 99.085 |
| 1.09 | 12.606 | 72.810 | 0.05683 | 5.159 | 0.00958 | - | 16.261 | 77.969 |
| 1.14 | 12.535 | 67.656 | 0.06492 | 2.233 | 0.01487 | - | 17.933 | 69.889 |
| 1.19 | 12.536 | 59.039 | 0.06688 | 4.162 | 0.18721 | - | 19.249 | 63.201 |
| 1.24 | 12.516 | 53.728 | 0.06572 | 4.968 | 1.1009 | - | 18.972 | 58.696 |
| 1.29 | 12.558 | 50.044 | 0.06321 | 3.536 | 1.9474 | - | 17.747 | 53.580 |
| 1.34 | 12.356 | 45.249 | 0.09968 | 4.648 | 2.474 | - | 23.152 | 49.897 |
| 1.39 | 12.514 | 36.839 | 0.07535 | 11.520 | 3.1427 | - | 50.079 | 48.359 |
| 1.44 | 12.554 | 27.166 | 0.06806 | 23.628 | 7.417 | - | 68.360 | 50.794 |
| 1.49 | 12.566 | 27.734 | 0.07787 | 18.465 | 8.1676 | 322.630 | 75.059 | 46.199 |
| 1.54 | 12.568 | 26.796 | 0.07641 | 17.759 | 5.0683 | 71.347 | 91.513 | 44.555 |
| 1.59 | 12.567 | 26.694 | 0.07622 | 15.791 | 3.4396 | 25.954 | 78.547 | 42.485 |
| 1.64 | 12.613 | 26.067 | 0.07632 | 12.265 | 2.7608 | 12.293 | 88.832 | 38.332 |
| 1.69 | 12.667 | 24.808 | 0.0740 | 7.3888 | 2.7221 | 6.751 | 112.23 | 32.196 |
| 1.74 | 12.742 | 22.974 | 0.07156 | 3.205 | 3.0837 | 4.750 | 128.61 | 26.179 |

Table S4. Summary of the impedance fitting data of $V_O$-$Co_3O_4$ electrode in 0.1 M KOH.

| Potential (V *vs.* RHE) | $R_S$ (Ω) | $R_p$ (Ω) | $CPE_p$ (mF) | $R_{film}$ (Ω) | $CPE_{film}$ (mF) | $R_{CT}$ (Ω) | $CPE_{CT}$ (mF) | $R_{total}$ (Ω) |
|---|---|---|---|---|---|---|---|---|
| 0.85 (OCP) | 12.683 | 74.309 | 0.07738 | 155.27 | 1.1185 | 1295.3 | 11.917 | 229.579 |
| 0.99 | 12.629 | 55.768 | 0.08354 | 78.001 | 1.2158 | - | 14.681 | 133.769 |
| 1.09 | 12.625 | 40.696 | 0.08327 | 42.406 | 2.0587 | - | 25.377 | 83.102 |
| 1.14 | 12.644 | 35.701 | 0.08621 | 26.224 | 3.1059 | - | 34.748 | 61.925 |
| 1.19 | 12.663 | 31.398 | 0.08802 | 15.778 | 3.4834 | - | 37.543 | 47.176 |
| 1.24 | 12.683 | 27.148 | 0.08783 | 10.6 | 3.813 | - | 36.894 | 37.748 |
| 1.29 | 12.703 | 22.77 | 0.08584 | 8.7596 | 4.4379 | - | 40.217 | 31.529 |
| 1.34 | 12.714 | 19.367 | 0.08741 | 7.2998 | 4.4395 | - | 49.664 | 26.666 |
| 1.39 | 12.722 | 15.89 | 0.08374 | 7.4598 | 5.3954 | - | 76.738 | 23.349 |
| 1.44 | 12.723 | 13.308 | 0.07905 | 7.5293 | 7.7775 | - | 131.99 | 20.837 |
| 1.49 | 12.71 | 11.478 | 0.07529 | 8.4753 | 11.351 | 124.18 | 151.61 | 19.953 |
| 1.54 | 12.693 | 11.226 | 0.08086 | 8.3745 | 10.565 | 23.942 | 135.11 | 19.601 |
| 1.59 | 12.736 | 11.163 | 0.08067 | 8.702 | 10.223 | 8.7998 | 148.25 | 19.865 |
| 1.64 | 12.82 | 11.202 | 0.08007 | 6.8221 | 7.5555 | 5.040 | 154.70 | 18.024 |
| 1.69 | 12.911 | 10.785 | 0.08069 | 5.2434 | 7.4826 | 2.682 | 201.45 | 16.028 |
| 1.74 | 12.965 | 10.411 | 0.08264 | 3.0072 | 6.3096 | 2.504 | 194.94 | 13.418 |

Table S5. Summary of the impedance fitting data for pure $Co_3O_4$ electrode in 0.1 M PBS.

| Potential (V *vs.* RHE) | $R_S$ (Ω) | $R_p$ (Ω) | $CPE_p$ (mF) | $R_{film}$ (Ω) | $CPE_{film}$ (mF) | $R_{CT}$ (Ω) | $CPE_{CT}$ (mF) | $R_{total}$ (Ω) |
|---|---|---|---|---|---|---|---|---|
| 0.955 | 11.332 | 251.98 | 0.17783 | 31.946 | 6.649 | - | 2.3133 | 283.926 |
| 1.055 | 11.429 | 218.53 | 0.10653 | 25.799 | 0.491 | - | 3.1269 | 244.329 |
| 1.105 | 11.471 | 197.52 | 0.11369 | 24.138 | 0.501 | - | 4.0174 | 221.658 |
| 1.155 | 11.486 | 176.21 | 0.10997 | 30.574 | 0.597 | - | 4.5054 | 206.784 |
| 1.205 | 11.486 | 153.71 | 0.18057 | 31.261 | 0.009 | - | 5.1697 | 184.971 |
| 1.255 | 11.47 | 130.82 | 0.11376 | 35.154 | 0.860 | - | 6.233 | 165.974 |
| 1.305 | 11.453 | 108.52 | 0.12122 | 42.967 | 0.900 | - | 7.5936 | 151.487 |
| 1.355 | 11.424 | 89.563 | 0.11981 | 44.702 | 0.975 | - | 9.453 | 134.265 |
| 1.405 | 11.407 | 71.402 | 0.26126 | 51.869 | 0.009 | - | 11.796 | 123.271 |
| 1.455 | 11.404 | 56.291 | 0.14335 | 46.912 | 1.461 | - | 14.324 | 103.203 |
| 1.505 | 11.406 | 38.782 | 0.14829 | 43.002 | 1.911 | - | 17.914 | 81.784 |
| 1.555 | 11.38 | 25.845 | 0.11751 | 17.826 | 5.234 | - | 29.445 | 43.671 |
| 1.605 | 11.376 | 18.044 | 0.10935 | 11.812 | 5.950 | 121.04 | 43.352 | 29.856 |
| 1.655 | 11.397 | 16.583 | 0.36408 | 7.2968 | 6.497 | 43.164 | 46.863 | 23.8798 |
| 1.705 | 11.44 | 15.523 | 0.10898 | 6.1883 | 6.801 | 22.165 | 50.354 | 21.7113 |
| 1.755 | 11.457 | 14.98 | 0.22284 | 4.2426 | 7.197 | 17.281 | 42.677 | 19.2226 |
| 1.805 | 11.484 | 14.107 | 0.10079 | 4.1525 | 6.367 | 12.597 | 52.499 | 18.2595 |
| 1.855 | 11.466 | 13.676 | 0.09352 | 3.5466 | 6.739 | 10.515 | 56.543 | 17.2226 |
| 1.905 | 11.509 | 13.292 | 0.0652 | 3.2196 | 9.351 | 8.2141 | 38.777 | 16.5116 |

Table S6. Summary of the impedance fitting data of $V_O$-$Co_3O_4$ electrode in 0.1 M PBS.

| Potential (V *vs.* RHE) | $R_S$ (Ω) | $R_p$ (Ω) | $CPE_p$ (mF) | $R_{film}$ (Ω) | $CPE_{film}$ (mF) | $R_{CT}$ (Ω) | $CPE_{CT}$ (mF) | $R_{total}$ (Ω) |
|---|---|---|---|---|---|---|---|---|
| 0.765 | 10.809 | 197.25 | 0.17783 | 92.1 | 6.649 | - | 2.3133 | 289.35 |
| 0.955 | 11.333 | 115.3 | 0.10653 | 67.668 | 0.49089 | - | 3.1269 | 182.968 |
| 1.055 | 11.2 | 100.39 | 0.11369 | 42.513 | 0.50081 | - | 4.0174 | 142.903 |
| 1.105 | 11.16 | 88.02 | 0.10997 | 36.295 | 0.59685 | - | 4.5054 | 124.315 |
| 1.155 | 10.888 | 72.724 | 0.18057 | 30.763 | 0.009 | - | 5.1697 | 103.487 |
| 1.205 | 11.087 | 65.191 | 0.11376 | 24.046 | 0.86041 | - | 6.233 | 89.237 |
| 1.255 | 11.043 | 55.969 | 0.12122 | 18.052 | 0.90031 | - | 7.5936 | 74.021 |
| 1.305 | 11.042 | 44.926 | 0.11981 | 16.577 | 0.97477 | - | 9.453 | 61.503 |
| 1.355 | 10.719 | 37.938 | 0.26126 | 13.124 | 0.009 | - | 11.796 | 51.062 |
| 1.405 | 10.958 | 31.819 | 0.14335 | 10.604 | 1.4606 | - | 14.324 | 42.423 |
| 1.455 | 10.941 | 25.024 | 0.14829 | 8.2081 | 1.9112 | - | 17.914 | 33.2321 |
| 1.505 | 11.012 | 18.381 | 0.11751 | 7.3074 | 5.2339 | - | 29.445 | 25.6884 |
| 1.555 | 11.165 | 15.543 | 0.10935 | 4.5332 | 5.9497 | - | 43.352 | 20.0762 |
| 1.605 | 10.821 | 12.455 | 0.36408 | 4.8789 | 6.497 | 134.71 | 46.863 | 17.3339 |
| 1.655 | 11.235 | 13.127 | 0.10898 | 3.8331 | 6.8014 | 48.116 | 50.354 | 16.9601 |
| 1.705 | 11.02 | 12.289 | 0.22284 | 1.9399 | 7.197 | 32.305 | 42.677 | 14.2289 |
| 1.755 | 11.274 | 12.341 | 0.10079 | 3.3143 | 6.3673 | 16.919 | 52.499 | 15.6553 |
| 1.805 | 11.338 | 11.784 | 0.09352 | 2.8679 | 6.7388 | 12.765 | 56.543 | 14.6519 |
| 1.855 | 10.897 | 8.5087 | 0.0652 | 0.46688 | 9.351 | 19.145 | 38.777 | 8.97558 |
| 1.905 | 10.735 | 7.6205 | 0.05085 | 0.13323 | 13.688 | 18.762 | 43.578 | 7.75373 |

Table S7. The relative ratio of surface $Co^{2+}$ and $Co^{3+}$ in pure $Co_3O_4$ and $V_O$-$Co_3O_4$ by Co 2p XPS spectral fitting.

| Potential (V *vs.* RHE) | The ratio of $Co^{2+}/Co^{3+}$ | Error (standard deviation) |
|---|---|---|
| Pure $Co_3O_4$ | 0.80142 | 0.00457 |
| 1.15 V | 0.79916 | 0.00596 |
| 1.25 V | 0.78617 | 0.0023 |
| 1.35 V | 0.78402 | 0.00483 |
| 1.45 V | 0.74536 | 0.01049 |
| 1.55 V | 0.71128 | 0.00806 |
| 1.65 V | 0.68745 | 0.00792 |
| 1.75 V | 0.68152 | 0.00198 |
| $V_O$-$Co_3O_4$ | 1.21771 | 0.00966 |
| 1.15 V | 1.17653 | 0.0057 |
| 1.25 V | 1.04209 | 0.00806 |
| 1.35 V | 1.00609 | 0.00449 |
| 1.45 V | 1.00765 | 0.007 |
| 1.55 V | 0.99391 | 0.00781 |
| 1.65 V | 1.0016 | 0.00321 |
| 1.75 V | 0.99416 | 0.00576 |

Table S8. The relative amount of surface oxygen vacancies in pure $Co_3O_4$ and $V_O$-$Co_3O_4$ by the ratio O2/O1 in O 1s XPS spectral fitting.

| Potential (V *vs.* RHE) | The ratio of O2/O1 | Error (standard deviation) |
|---|---|---|
| Pure $Co_3O_4$ | 0.66113 | 0.00661 |
| 1.15 V | 0.63479 | 0.02085 |
| 1.25 V | 0.64535 | 0.01894 |
| 1.35 V | 0.56494 | 0.00479 |
| 1.45 V | 0.60319 | 0.03392 |
| 1.55 V | 0.60738 | 0.02989 |
| 1.65 V | 0.59255 | 0.01467 |
| 1.75 V | 0.67916 | 0.01115 |
| $V_O$-$Co_3O_4$ | 5.40852 | 0.21657 |
| 1.15 V | 3.7367 | 0.47707 |
| 1.25 V | 2.46678 | 0.20227 |
| 1.35 V | 1.79818 | 0.06114 |
| 1.45 V | 1.15082 | 0.03206 |
| 1.55 V | 1.12923 | 0.04399 |
| 1.65 V | 1.0981 | 0.02825 |
| 1.75 V | 1.02168 | 0.0257 |

Note: It would reasonable to assume that the size of the catalysts was no obvious change, such as shown in SEM/TEM images. The change of the ratio of O2/O1 could be approximately associated to the effect of applied potential in *quasi-operando* XPS characterization. So, we use of the ratio O2/O1 as one of yardstick to estimate the relative amount of surface oxygen vacancies.

Table S9. Summary of the FT-EXAFS fitting data for pure $Co_3O_4$ and $V_O$-$Co_3O_4$ carried out the critical potential.

| Samples | Path | CN | R (Å) | $\sigma^2$(Å$^2$) | $\Delta E_0$(eV) | *R*-factor |
|---|---|---|---|---|---|---|
| $Co_3O_4$ (theory) | Co-O | 5.3 | 1.915 | | | |
| | Co-$Co_{(Oh)}$ | 4 | 2.854 | | | |
| | Co-$Co_{(Td)}$ | 8 | 3.357 | | | |
| Pure $Co_3O_4$ (OCP) | Co-O | 4.09497 ± 0.81899 | 1.91536 ± 0.03831 | 0.00061 ± 0.00012 | 4.499 ± 0.8998 | |
| | Co-$Co_{(Oh)}$ | 4.1566 ± 0.83132 | 2.85734 ± 0.05715 | 0.0035 ± 0.0007 | 3.988 ± 0.7976 | 0.0014656 |
| | Co-$Co_{(Td)}$ | 6.69541 ± 1.33908 | 3.36824 ± 0.06736 | 0.00566 ± 0.00113 | 3.988 ± 0.7976 | |
| Pure $Co_3O_4$ (1.15 V) | Co-O | 4.08819 ± 0.81764 | 1.91431 ± 0.03829 | 0.00063 ± 0.00013 | 4.386 ± 0.8772 | |
| | Co-$Co_{(Oh)}$ | 4.21672 ± 0.84334 | 2.86435 ± 0.05729 | 0.00386 ± 0.00077 | 4.7 ± 0.94 | 0.0016130 |
| | Co-$Co_{(Td)}$ | 6.34223 ± 1.26845 | 3.37341 ± 0.06747 | 0.0055 ± 0.0011 | 4.7 ± 0.94 | |
| Pure $Co_3O_4$ (1.25 V) | Co-O | 4.13834 ± 0.82767 | 1.91551 ± 0.03831 | 0.0007 ± 0.00014 | 4.49 ± 0.898 | |
| | Co-$Co_{(Oh)}$ | 4.2616 ± 0.85232 | 2.86112 ± 0.05722 | 0.00344 ± 0.00069 | 4.432 ± 0.8864 | 0.0008914 |
| | Co-$Co_{(Td)}$ | 6.43098 ± 1.2862 | 3.37207 ± 0.06744 | 0.00541 ± 0.00108 | 4.432 ± 0.8864 | |
| Pure $Co_3O_4$ (1.35 V) | Co-O | 4.108192 ± 0.82164 | 1.91424 ± 0.03828 | 0.00064 ± 0.00013 | 4.428 ± 0.8856 | |
| | Co-$Co_{(Oh)}$ | 4.25883 ± 0.85177 | 2.85896 ± 0.05718 | 0.00351 ± 0.0007 | 4.149 ± 0.8298 | 0.0014851 |
| | Co-$Co_{(Td)}$ | 6.61122 ± 1.32224 | 3.36814 ± 0.06736 | 0.00546 ± 0.00109 | 4.149 ± 0.8298 | |
| Pure $Co_3O_4$ (1.45 V) | Co-O | 4.21781 ± 0.84356 | 1.91383 ± 0.03828 | 0.00097 ± 0.00019 | 4.45 ± 0.89 | |
| | Co-$Co_{(Oh)}$ | 4.18328 ± 0.83666 | 2.85591 ± 0.05712 | 0.00342 ± 0.00068 | 3.844 ± 0.7688 | 0.0009543 |
| | Co-$Co_{(Td)}$ | 6.67975 ± 1.33595 | 3.36479 ± 0.0673 | 0.00553 ± 0.00111 | 3.844 ± 0.7688 | |
| Pure $Co_3O_4$ (1.55 V) | Co-O | 4.37832 ± 0.87566 | 1.91537 ± 0.03831 | 0.00059 ± 0.00012 | 4.829 ± 0.9658 | |
| | Co-$Co_{(Oh)}$ | 4.86555 ± 0.97311 | 2.86455 ± 0.05729 | 0.00435 ± 0.00087 | 5.105 ± 1.021 | 0.0007652 |
| | Co-$Co_{(Td)}$ | 6.36856 ± 1.27371 | 3.37638 ± 0.06753 | 0.00462 ± 0.00092 | 5.105 ± 1.021 | |
| Pure $Co_3O_4$ (1.65 V) | Co-O | 4.52515 ± 0.90503 | 1.87208 ± 0.03744 | 0.00321 ± 0.00064 | -3.263 ± 0.6526 | |
| | Co-$Co_{(Oh)}$ | 3.34606 ± 0.66921 | 2.83649 ± 0.05673 | 0.00157 ± 0.00031 | 1.517 ± 0.3034 | 0.0025734 |
| | Co-$Co_{(Td)}$ | 6.61924 ± 1.32385 | 3.3487 ± 0.06697 | 0.00157 ± 0.00031 | 1.517 ± 0.3034 | |
| Pure $Co_3O_4$ (1.75 V) | Co-O | 4.08391 ± 0.81678 | 1.89849 ± 0.03797 | 0.00003 ± 0.00001 | 3.313 ± 0.6626 | |
| | Co-$Co_{(Oh)}$ | 3.70337 ± 0.74067 | 2.84079 ± 0.05682 | 0.00395 ± 0.00079 | 0.386 ± 0.0772 | 0.0019727 |
| | Co-$Co_{(Td)}$ | 6.93396 ± 1.38679 | 3.34431 ± 0.06689 | 0.01052 ± 0.0021 | 0.386 ± 0.0772 | |
| $V_O$-$Co_3O_4$ (OCP) | Co-O | 3.16921 ± 0.63384 | 1.91075 ± 0.03821 | 0.00011 ± 0.00002 | 3.361 ± 0.6722 | 0.0013688 |
| | Co-$Co_{(Oh)}$ | 3.72149 ± 0.7443 | 2.86862 ± 0.05737 | 0.0041 ± 0.00082 | 5.052 ± 1.0104 | |

| | | | | | | |
|---|---|---|---|---|---|---|
| | Co-$Co_{(Td)}$ | 4.53574 ± 0.90715 | 3.37746 ± 0.06755 | 0.00439 ± 0.00088 | 5.052 ± 1.0104 | |
| $V_O$-$Co_3O_4$ (1.15 V) | Co-O | 3.38392 ± 0.67678 | 1.91504 ± 0.0383 | 0.00047 ± 0.00009 | 4.546 ± 0.9092 | |
| | Co-$Co_{(Oh)}$ | 3.61875 ± 0.72375 | 2.85619 ± 0.05712 | 0.00315 ± 0.00063 | 3.695 ± 0.739 | 0.0009590 |
| | Co-$Co_{(Td)}$ | 5.81167 ± 1.16233 | 3.36367 ± 0.06727 | 0.00545 ± 0.00109 | 3.695 ± 0.739 | |
| $V_O$-$Co_3O_4$ (1.25 V) | Co-O | 3.46935 ± 0.69387 | 1.91276 ± 0.03826 | 0.00009 ± 0.00002 | 4.391 ± 0.8782 | |
| | Co-$Co_{(Oh)}$ | 3.62443 ± 0.72489 | 2.85631 ± 0.05713 | 0.00314 ± 0.00063 | 3.885 ± 0.777 | 0.0016365 |
| | Co-$Co_{(Td)}$ | 6.02823 ± 1.20565 | 3.36598 ± 0.06732 | 0.00585 ± 0.00117 | 3.885 ± 0.777 | |
| $V_O$-$Co_3O_4$ (1.35 V) | Co-O | 3.54966 ± 0.70993 | 1.90747 ± 0.03815 | 0.0004 ± 0.00008 | 3.465 ± 0.693 | |
| | Co-$Co_{(Oh)}$ | 3.39479 ± 0.67896 | 2.85117 ± 0.05702 | 0.00001 ± 0.00001 | 4.111 ± 0.8222 | 0.0020942 |
| | Co-$Co_{(Td)}$ | 7.25442 ± 1.45088 | 3.33751 ± 0.06675 | 0.00648 ± 0.0013 | 4.111 ± 0.8222 | |
| $V_O$-$Co_3O_4$ (1.45 V) | Co-O | 3.69484 ± 0.73897 | 1.90979 ± 0.0382 | 0.00055 ± 0.00011 | 4.146 ± 0.8292 | |
| | Co-$Co_{(Oh)}$ | 3.36427 ± 0.67285 | 2.85607 ± 0.05712 | 0.00233 ± 0.00047 | 3.639 ± 0.7278 | 0.0032281 |
| | Co-$Co_{(Td)}$ | 5.59719 ± 1.11944 | 3.36003 ± 0.0672 | 0.00491 ± 0.00098 | 3.639 ± 0.7278 | |
| $V_O$-$Co_3O_4$ (1.55 V) | Co-O | 3.43014 ± 0.68603 | 1.91546 ± 0.03831 | 0.00014 ± 0.00003 | 4.717 ± 0.9434 | |
| | Co-$Co_{(Oh)}$ | 3.80138 ± 0.76028 | 2.85786 ± 0.05716 | 0.00351 ± 0.00071 | 4.058 ± 0.8116 | 0.0011548 |
| | Co-$Co_{(Td)}$ | 5.49308 ± 1.09862 | 3.36767 ± 0.06735 | 0.00512 ± 0.00102 | 4.058 ± 0.8116 | |
| $V_O$-$Co_3O_4$ (1.65 V) | Co-O | 3.38384 ± 0.67677 | 1.91367 ± 0.03827 | 0.0001 ± 0.00002 | 4.598 ± 0.9196 | |
| | Co-$Co_{(Oh)}$ | 3.72801 ± 0.7456 | 2.85834 ± 0.05717 | 0.00338 ± 0.00068 | 4.164 ± 0.8328 | 0.0011833 |
| | Co-$Co_{(Td)}$ | 5.56136 ± 1.11227 | 3.36804 ± 0.06736 | 0.00558 ± 0.00112 | 4.164 ± 0.8328 | |
| $V_O$-$Co_3O_4$ (1.75 V) | Co-O | 3.56082 ± 0.71216 | 1.91451 ± 0.03829 | 0.00026 ± 0.00005 | 4.67 ± 0.934 | |
| | Co-$Co_{(Oh)}$ | 3.50438 ± 0.70088 | 2.85767 ± 0.05715 | 0.00291 ± 0.00058 | 4.058 ± 0.8116 | 0.0018739 |
| | Co-$Co_{(Td)}$ | 5.40799 ± 1.0816 | 3.36585 ± 0.06732 | 0.00508 ± 0.00102 | 4.058 ± 0.8116 | |

EXAFS analysis: Data merging, background subtraction, normalization and fitting of the XANES and EXAFS spectra were performed using Demeter software packagei.[8] Simulation results for the fits of the $k^3$-weighted EXAFS spectra of $Co_3O_4$ nanosheets as a function of catalyst state. Fitting of the $k^3$-weighted data was done in k-space between 2.85 and 11.85 $Å^{-1}$ using a Hanning-shaped window. The amplitude-reduction factor $S_0^2$ was defined at 0.8. The R-ranges for the fitting of all the EXAFS data were set as 1.15-3.52 Å. We performed EXAFS curve fitting for the spinel oxides by referencing a landmark work.[9-12] The coordination numbers (CN), the distances (R) and Debye-Waller factors (σ) were determined independently. The quality of the fitting was evaluated by the R-factor (Rf). The fitting results that determined by the scattering of the photoexcited electron by neighbor atoms and returning back to the absorber atom, are estimated to be: coordination number N (±20%), distance R (±2%) (Å), potential correction $\Delta E_0$ (±20%), and Debye-Waller factor $\Delta\sigma^2$ (±20%).

Reference

1. L. Xu, Q. Jiang, Z. Xiao, X. Li, J. Huo, S. Wang and L. Dai, Angewandte Chemie International Edition, **2016**, *55*, 5277-5281.

2. S. Dou, L. Tao, J. Huo, S. Wang and L. Dai, Energy & Environmental Science, **2016**, *9*, 1320-1326.

3. Z. Xiao, X. Huang, L. Xu, D. Yan, J. Huo and S. Wang, Chemical communications, **2016**, *52*, 13008-13011.

4. J. Li, Y. Wang, T. Zhou, H. Zhang, X. Sun, J. Tang, L. Zhang, A. M. Al-Enizi, Z. Yang, G. Zheng, Journal of the American Chemical Society, **2015**, 137, 14305-14312.

5. McCrory, C. C. L.; Jung, S.; Peters, J. C.; Jaramillo, T. F, Journal of the American Chemical Society, **2013**, 135, 16977-16987.

6. R. Doyle and M. Lyons, Journal of The Electrochemical Society, **2013**, *160*, H142-H154.

7. J. Li, H.-X. Liu, W. Gou, M. Zhang, Z. Xia, S. Zhang, C.-R. Chang, Y. Ma and Y. Qu, Energy & Environmental Science, **2019**, *12*, 2298-2304.

8. B. Ravel and M. Newville, Journal of Synchrotron Radiation, **2005**, *12*, 537-541.

9. S. Sun, Y. Sun, Y. Zhou, S. Xi, X. Ren, B. Huang, H. Liao, L. P. Wang, Y. Du and Z. Xu, Angewandte Chemie International Edition, **2019**, *58*, 6042-6047.

10. R. R. Zhang, Y. C. Zhang, L. Pan, G. Q. Shen, N. Mahmood, Y. H. Ma, Y. Shi, W. Y. Jia, L. Wang, X. W. Zhang, W. Xu and J. J. Zou, ACS Catalysis, **2018**, *8*, 3803-3811.

11. A. Bergmann, T. E. Jones, E. M. Moreno, D. Teschner, P. Chernev, M. Gliech, T. Reier, H. Dau and P. Strasser, Nature Catalysis, **2018**, *1*, 711-719.

12. A. Bergmann, E. Martinez-Moreno, D. Teschner, P. Chernev, M. Gliech, J. F. de Araujo, T. Reier, H. Dau and P. Strasser, Nature communications, **2015**, *6*, 8625.